

Contents lists available at ScienceDirect

# Journal of Catalysis

journal homepage: www.elsevier.com/locate/jcat



# Catalytic hydrogenation of furfural to furfuryl alcohol on hydrotalcite-derived $Cu_xNi_{3-x}AlO_v$ mixed-metal oxides



Lin Luo<sup>a</sup>, Fulong Yuan<sup>a</sup>, Francisco Zaera<sup>b,\*</sup>, Yujun Zhu<sup>a,\*</sup>

- <sup>a</sup> Key Laboratory of Functional Inorganic Material Chemistry (Heilongjiang University), Ministry of Education, School of Chemistry and Materials, Heilongjiang University, Harbin 150080, PR China
- b Department of Chemistry and UCR Center for Catalysis, University of California, Riverside, 900 University Avenue, Riverside, CA 92521, United States

#### ARTICLE INFO

Article history: Received 24 August 2021 Revised 6 October 2021 Accepted 7 October 2021 Available online 16 October 2021

Keywords: Cu<sub>x</sub>Ni<sub>3-x</sub>AlO<sub>y</sub> oxides In-situ reduction Cu<sup>0</sup> species Selective hydrogenation of furfural

#### ABSTRACT

It is highly desirable but quite challenging to replace precious metals with cheaper elements in the catalytic selective hydrogenation of unsaturated aldehydes. Herein, we report the preparation of a series of  $Cu_xNi_{3-x}AlO_y$  mixed-metal oxides (x = 0.5, 1, 2) derived from  $Cu_xNi_{3-x}Al$  hydrotalcite to be used as catalysts for the promotion of the selective hydrogenation of furfural (FAL) to furfuryl alcohol (FOL). It was found that the catalyst with the  $Cu_2Ni_1AlO_y$  stoichiometry exhibited the best performance, with 98% FAL conversion and 99% selectivity toward FOL after 1.5 h at 120 °C and under a  $H_2$  pressure of 1.6 MPa, and also good reusability. On the basis of the combined results from catalyst characterization studies using XRD,  $H_2$ -TPR, TEM, XPS, and in-situ FT-IR, it was concluded that the  $CuO_x$  species on the surface of the  $Cu_xNi_{3-x}AlO_y$  catalysts can be reduced in situ to metallic copper during reaction, and that this  $Cu^0$  species is likely the responsible for the adsorption and conversion of FAL. The addition of Ni to these mixed-metal oxides helps disperse the Cu phase and hence make it easier to reduce and activate. It may also be that NiO can promote  $H_2$  dissociation to aid with the hydrogenation catalysis. Our work advances a new strategy for the design of simple, cheap, and efficient catalysts for the hydrogenation of FAL to FOL.

© 2021 Elsevier Inc. All rights reserved.

#### 1. Introduction

In a quest for clean and pollution-free energy sources, biomass has become a promising candidate [1–3]. Some work has been aimed at the use of biomass for direct energy generation, but additional interest has been directed at using specific building blocks from biomass to produce other chemical of interest. Furfural (FAL) in particular is an important platform compound derived from lignocellulose that can be further converted into various non-petroleum valuable chemicals such as methylfuran, methyltetrahydrofuran, valerate esters, and ethylfurfuryl and ethyltetrahydrofurfuryl ethers [4,5]. These compounds are in turn used for the direct or indirect synthesis of a variety of chemical products used as pharmaceuticals and pesticides, and in other fine chemicals applications [6,7].

Furfuryl alcohol (FOL) is one of the most desirable products from the selective hydrogenation of FAL (Scheme S1). Numerous monometallic and bimetallic catalysts have been tested for this process, including catalysts based on Ru, Pd, Pt, Ni, Cu, Pd-Cu and Pt-Cu [8–11], but, to date, those mostly include at least one noble

metal. Indeed, Pt-based catalysts have been widely used in the selective hydrogenation of unsaturated aldehydes in general because of their excellent catalytic activity under mild reaction conditions [12–17]. Unfortunately, those metals are scare and costly; it would be desirable to find alternative materials for these processes.

In recent years, some non-noble metal catalysts have been successfully tested for the hydrogenation of FAL to FOL, the most common of which are Ni- and Cu-based. Although Ni-based catalysts exhibit relatively good catalytic performance [18–20], there are some issues that limit their application: metallic Ni is too active and tend to dehydrogenate and decompose the reactants, and it is difficult to store the catalyst in a way that avoids its oxidation. Cu-based catalysts such as  $\text{CuCr}_2\text{O}_4$  show good activity as well, but are not environmentally safe due to the poisonous nature of the Cr species. In order to get around this problem, researchers have tried chromium-free Cu-based catalysts such as Cu/C[21],  $\text{Cu/Al}_2\text{O}_3$  [22] and  $\text{CuAl}_2\text{O}_4$  [23], but on the whole, the catalytic efficiency of those Cu-based catalysts has proven to be low. Effectively improving the catalytic efficiency of Cu-based catalysts still remains a challenge.

Another problem is that both Ni- and Cu-based catalysts require relatively harsh conditions such as high reaction temperatures and

<sup>\*</sup> Corresponding authors. E-mail addresses: zaera@ucr.edu (F. Zaera), yujunzhu@hlju.edu.cn (Y. Zhu).

H<sub>2</sub> pressures for their operation, adding to the operational cost of the process and incorporating certain safety hazards. Moreover, most of the catalysts developed so far require pre-reduction treatments, which not only prolong the reaction process but also consume energy. Prior to this, there were some reports on the use of Cu-Ni alloy catalysts in the selective hydrogenation of furfural [24–26]. Facts have shown that the formation of Cu-Ni bimetallic alloy catalysts is indeed beneficial to the improvement of catalytic activity compared to Cu or Ni single-metal catalysts, but the conditions for forming alloys are relatively harsh. With that in mind, the primary goal of this work has been to design a catalyst based on unalloyed non-noble metals with high catalytic efficiency and operability for catalytic hydrogenations under relatively mild reaction conditions.

Several steps are involved in the hydrogenation of carbonyl-containing products such as FAL, and it is not always easy to find a simple catalytic phase that can promote all in an optimal way. For selective hydrogenations in particular, there is a need to have one type of sites that efficiently dissociate hydrogen molecules to produce adsorbed hydrogen atoms and another that helps incorporate those H atoms into the unsaturated bonds of the reactant in a selective way. Single atom alloy (SAA) catalysts, where an active diluted metal such as Pt is used for the H<sub>2</sub> activation and a second, milder, metal such as Cu is employed to carry out the hydrogenation steps, have proven a promising solution [14,27]. However, in the case of Cu- and Ni- based catalysts, oxidation of the surface is always a potential issue. For catalysts inspired on the SAA idea to be successful, a way to stabilize the active metallic phase is required.

Inspired by these ideas, a series of Cu<sub>x</sub>Ni<sub>3-x</sub>AlO<sub>y</sub> mixed-metal oxides (MMO) derived from hydrotalcite were designed and developed for the hydrogenation of FAL to FOL. It was found that with such catalysts the reaction can be operated under relatively mild reaction conditions, and that the catalyst can be used as prepared, without any pre-treatment. With the aid of results from using various experimental characterization techniques, a reaction process is proposed where highly dispersed CuO species on the surface of the catalyst can be reduced in situ to form and stabilize the Cu<sup>0</sup> species that adsorb and selectively hydrogenate FAL to FOL.

# 2. Experimental

#### 2.1. Materials

Copper (II) nitrate trihydrate (Cu(NO<sub>3</sub>)<sub>2</sub>·3H<sub>2</sub>O) was purchased from Basf Chemical Limited Company (Tianjin, China). Nickel (II) nitrate hexahydrate (Ni(NO<sub>3</sub>)<sub>2</sub>·6H<sub>2</sub>O) and FAL were obtained from Guangfu Fine Chemical Research institute (Tianjin, China). Aluminum nitrate nonahydrate (Al(NO<sub>3</sub>)<sub>3</sub>·9H<sub>2</sub>O) was bought from Kemiou Chemical Reagent Co. Ltd. (Tianjin, China). Sodium carbonate anhydrous (Na<sub>2</sub>CO<sub>3</sub>) and 1-octanol were got from Tianli Chemical Reagent (Tianjin, China). Sodium hydroxide (NaOH) was purchased from Tianda Chemical Reagent Factory (Tianjin, China). Isopropanol was purchased from Fuyu Fine Chemical Reagent (Tianjin, China). FOL was obtained from Zhanyun Chemical Reagent (Shanghai, China). All of them were of analytical grade purity and used as received without further purification.

# 2.2. Catalysts preparation

The  $Cu_xNi_{3-x}Al$ -LDH (layered double hydroxides) aluminumonly hydrotalcites were synthesized by a co-precipitation method. Typically,  $Cu(NO_3)_2 \cdot 3H_2O$ ,  $Ni(NO_3)_2 \cdot 6H_2O$  and  $Al(NO_3)_3 \cdot 9H_2O$  were dissolved in 100 mL deionized water in 0:3:1, 0.5:2.5:1, 1:2:1, 2:1:1 or 3:0:1 Cu/Ni/Al molar ratios (for x=0, 0.5, 1, 2, and 3, respectively) and total metal concentration of 0.15 mol/L to get the initial Solution A. NaOH and Na<sub>2</sub>CO<sub>3</sub> were dissolved in 100 mL deionized water to get Solution B, in which the molar concentration of NaOH is 1.8 times that of all metal cations, and the molar concentration of Na<sub>2</sub>CO<sub>3</sub> is twice that of Al<sup>3+</sup>. Solution B was then added slowly into Solution A while stirring at 500 rpm until the pH value of the mixed solution reached 9.5  $\pm$  0.2. The resulting suspension was aged at room temperature for 24 h, then filtered and washed several times with deionized water until the pH of the filtrate was 7.0. The resulting precipitate was dried at 80 °C overnight to obtain the Cu<sub>x</sub>Ni<sub>3-x</sub>Al-LDH hydrotalcites. They were put in crucibles and calcined to 500 °C for 4 h at a heating rate of 2 °C/min under air to obtain the final Cu<sub>x</sub>Ni<sub>3-x</sub>AlO<sub>y</sub> mixed-metal oxides which we here denote as Cu<sub>x</sub>Ni<sub>3-x</sub>AlO<sub>y</sub> (x = 0, 0.5, 1, 2, 3) according to their Cu/Ni/Al molar ratio.

#### 2.3. Catalyst characterization

The X-ray diffraction (XRD) measurements were performed on a Rigaku D/max - IIIB diffractometer using a Cu K $\alpha$  radiation ( $\lambda$  = 1. 5418 Å) source operated at 40 kV and 20 mA. The patterns were recorded from  $2\theta$  = 5° to  $2\theta$  = 80° at steps of 0.02°. The N<sub>2</sub> adsorption desorption isothermals were measured at 77 K using a Micrometrics Tristar II 3020 analyzer, and the specific surface areas were calculated using the Brunauer-Emmett-Teller (BET) method. The samples were degassed under vacuum at 150 °C for 8 h before analysis. X-ray photoelectron spectroscopy (XPS) and Auger electron spectroscopy (AES) data were acquired using a Kratos-AXIS ULTRA DLD system with a monochromatic Al K $\alpha$  X-rays source. All binding energies (BEs) were referenced to a C 1s BE value of 284.6 eV for adventitious carbon. The contents of Cu, Ni and Al were determined by inductively coupled plasma-optical emission spectrometry (ICP-OES), using a PerkinElmer Optima 7000DV analyzer. Before each ICP-OES test, a weighted amount of the sample was dissolved in aqua regia and diluted with water. Transmission electron microscopy (TEM) analysis was carried out on a JEOL model JEM-2100 electron microscope with an acceleration voltage of 200 kV.

Two types of  $H_2$  temperature programmed reduction ( $H_2$ -TPR) experiments were performed on a Tianjin XQ TP5080 instrument with a thermal conductivity detector (TCD), with fresh and onceused samples, respectively. In a typical  $H_2$ -TPR experiment, 20 mg catalyst was first pretreated at either 300 or 120 °C for 30 min and in a stream of either  $O_2$  (fresh sample) or He (the sample used once) flowing at a rate of 30 mL/min and then cooled down to 30 °C under the same conditions. Afterward, the sample was heated from 30 °C to 800 °C at a rate of 10 °C/min in a stream of 5%  $H_2/N_2$  gas at a rate of 30 mL/min.

The dispersion of Cu was measured by a reduction-oxidation-reduction method. First, 20 mg of fresh catalyst was pretreated for 30 min at 120 °C in a He atmosphere and then cooled to room temperature in the same He gas in order to remove water and other impurities adsorbed on the surface. Afterward, the sample was heated from 30 °C to 350 °C at a rate of 10 °C/min in a stream of 5%  $\rm H_2/N_2$  gas with a flow of 30 mL/min, then cooled down to room temperature (during which the  $\rm H_2$  consumption was recorded as  $\rm A_1$ ). Third, the catalyst was oxidized with 0.8%  $\rm N_2O/N_2$  gas at 50 °C for 1 h and then cooled down to room temperature. Finally, the sample was heated from 30 °C to 350 °C at a rate of 10 °C/min in 5%  $\rm H_2/N_2$  gas with a flow of 30 mL/min and then cooled to room temperature (during which the  $\rm H_2$  consumption is recorded as  $\rm A_2$ ). The Cu dispersion was calculated by using the formula:

Cu dispersion = 
$$[2A_2/A_1] \times 100\%$$
 (1)

In situ FT-IR measurements of FAL adsorption were performed using a Nicolet 6700 FTIR spectrometer equipped with a diffuse reflectance (DRIFT) cell (Harrick) and a mercury-cadmium-telluride (MCT) detector cooled by liquid  $N_2$ . The samples were first purged in  $N_2$  at 200 °C for 30 min. After cooling to 25 °C under a continuous flow of  $N_2$ , a DRIFT background spectrum was collected. Subsequently, FAL was introduced into the cell at 25 °C with the aid of a stream of  $N_2$ : the surfaces of the catalysts were exposed to the vapor of FAL carried out by the  $N_2$  stream for 60 min, after which the cell was purged with pure  $N_2$  for another 30 min to remove any physisorbed FAL. Finally, a second DRIFT spectrum was collected. The final traces were obtained by ratioing the second (sample) spectrum by the first (background). 32 scans were added during the acquisition of each spectrum.

## 2.4. Hydrogenation of FAL to FOL

Catalytic FAL hydrogenation runs were performed in a 100 mL stainless steel high-pressure reactor with a Telfon liner. The catalyst (0.0500 g), furfural (0.2525 g) and isopropanol (15 mL) were loaded into the reactor, and the mixture was purged five times with H<sub>2</sub> after sealing the reactor volume to remove any residual air trapped inside the reactor. The reactor was first filled with some  $H_2$  and heated to the predetermined temperature (80–140 °C), after which the H<sub>2</sub> was adjusted to the final desired pressure (1.0-1.8 MPa). After reactions, the reactor was cooled down to room temperature in water, and the liquid products were analyzed by gas chromatography (BFRL SP-3420A, China) using a HP-5 column (30 m  $\times$  0.32 mm  $\times$  0.25  $\mu$ m) and a flame ionization detector (FID). A fixed small amount of 1-octanol was added to the liquid samples as an external standard. In the recyclability tests, the catalyst was reused after washing it with isopropanol and water and drying it overnight in a vacuum oven. Catalytic activities were estimated in terms of furfural consumption rates using the formula

$$Reactioncrate = \frac{\left\{ [\mathit{FAL}]_0 - [\mathit{FAL}]_t \right\} \times V}{m_{\mathit{Catalyst}} \times t} \tag{2}$$

where  $[FAL]_0$  and  $[FAL]_t$  correspond to the initial concentration of furfural and that at reaction time t (h), respectively; V represents the solution volume, and  $m_{Catalyst}$  represents the mass of the catalyst. An experimental error of less than  $\pm$  5% was estimated in all the activity tests. Turnover frequency (TOF) was here defined by equation (3) [29]:

$$TOF = \frac{FOL_{yielded}}{t(m_{catalyst}X/M)D}$$
 (3)

Where  $FOL_{yielded}$  is the amount of FOL produced (in moles), t is the reaction time (h),  $m_{catalyst}$  is the amount of catalyst (g), X is the Cu content in the catalyst (wt.%), D is the Cu dispersion (%), and M is the molar weight of Cu (M = 63.5 g/mol).

#### 3. Results and discussion

# 3.1. Textural properties

A series of  $Cu_xNi_{3-x}AlO_y$  (x=0,0.5,1,2,3) mixed-oxide catalysts was prepared by using the corresponding  $Cu_xNi_{3-x}Al-LDH$  hydrotalcite compounds as precursors. As displayed in Table 1, the actual Cu/Ni/Al atomic ratios in the  $Cu_xNi_{3-x}AlO_y$  catalysts measured by ICP are quite close to their corresponding theoretical value.

The XRD patterns of all  $Cu_xNi_{3-x}Al$ -LDH precursors, shown in Fig. S1, display characteristic diffraction peaks at  $2\theta = 11.5, 23.1, 35.0, 39.2, 47.5, 61.1, and <math>62.4^\circ$ , which are identified here as corre-

sponding to the (003), (006), (012), (015), (018), (110), and (113) crystal planes of hydrotalcite-like compound (ICPDS 15-0087/37-0630) [30], respectively. The XRD patterns of Ni<sub>3</sub>AlO<sub>v</sub> and Cu<sub>3</sub>AlO<sub>v</sub>, on the other hand, present characteristic diffractions peaks at  $2\theta$  = 37.5, 43.5 and 63.5°, belonging to the NiO phase (JCPDS 75-0197), and at  $2\theta$  = 35.5, 38.8 and 48.7°, associated with the CuO phase (JCPDS 89-5899) (Fig. 1A). It is noteworthy that only characteristic diffraction peaks for NiO, and not CuO, are observed with Cu<sub>0.5</sub>Ni<sub>2.5</sub>AlO<sub>v</sub> and Cu<sub>1</sub>Ni<sub>2</sub>AlO<sub>v</sub>, indicating that CuO species, if present in those catalysts, are either highly dispersed or in noncrystalline form. On the other hand, mixed phases of CuO and NiO are clearly observed in the XRD patterns of Cu<sub>2</sub>Ni<sub>1</sub>AlO<sub>v</sub>. Moreover, the intensity of the diffraction peaks attributed to NiO decreases gradually with increasing Cu content. The XPS results reported in Fig. S2 indicate that both Cu and Ni in the fresh catalyst are mainly in oxidized (CuO and NiO) form, consistent with the XRD results.

Results from isothermal  $N_2$  adsorption-desorption experiments on the  $Cu_xNi_{3-x}AlO_y$  samples show a typical IV isotherm shape with an H2 hysteresis loop, except for the  $Cu_3AlO_y$  sample, which displays an H3 hysteresis loop instead (Fig. 1B); the latter may reflect a different pore shape after calcination. As displayed in Fig. 1C, the pore diameter of all samples calculated from those isotherms cover a range from 2 nm to 50 nm, as expected from mesoporous structures derived from nanoparticles accumulation. The BET surface areas were found to increase in the Cu-Ni mixed-oxide samples with increasing Ni content, but to decrease slightly for the Ni-only sample (Table 1).

#### 3.2. Catalyst reducibility

H<sub>2</sub>-TPR experiments were carried out to evaluate the reducibility of the Cu<sub>x</sub>Ni<sub>3-x</sub>AlO<sub>y</sub> catalysts; the results are displayed in Fig. 1D. For Ni<sub>3</sub>AlO<sub>v</sub>, only one wide reduction peak is observed around 525 °C, associated with the reduction of the NiO species [31]. With the Cu<sub>x</sub>Ni<sub>3-x</sub>AlO<sub>y</sub> and Cu<sub>3</sub>AlO<sub>y</sub> catalysts, by contrast, several peaks are seen below 320 °C, assigned to the progressive reduction of the CuO species to Cu<sup>0</sup> [32,33]; the low-temperature (214/218 °C) peak is attributed to the reduction of highly dispersed surface CuO species on the catalyst, whereas the feature seen at medium temperatures (about 225-247 °C) may be associated with reduction of CuO clusters, and the peak at higher temperatures (>270 °C) to the reduction of crystallized CuO species. Specifically, with Cu<sub>0.5</sub>Ni<sub>2.5</sub>AlO<sub>v</sub>, only reduction of highly dispersed surface CuO is seen, at 214 °C (together with a peak at 480 °C due to reduction of NiO species). As the copper content increases, the CuO reduction peak shifts to high temperatures and becomes broader, suggesting the formation of CuO clusters, and even some crystallization. These results are in good agreement with the XRD results (Fig. 1A), and suggest that the mixed NiO phase may help with the reduction and dispersion of the Cu phase.

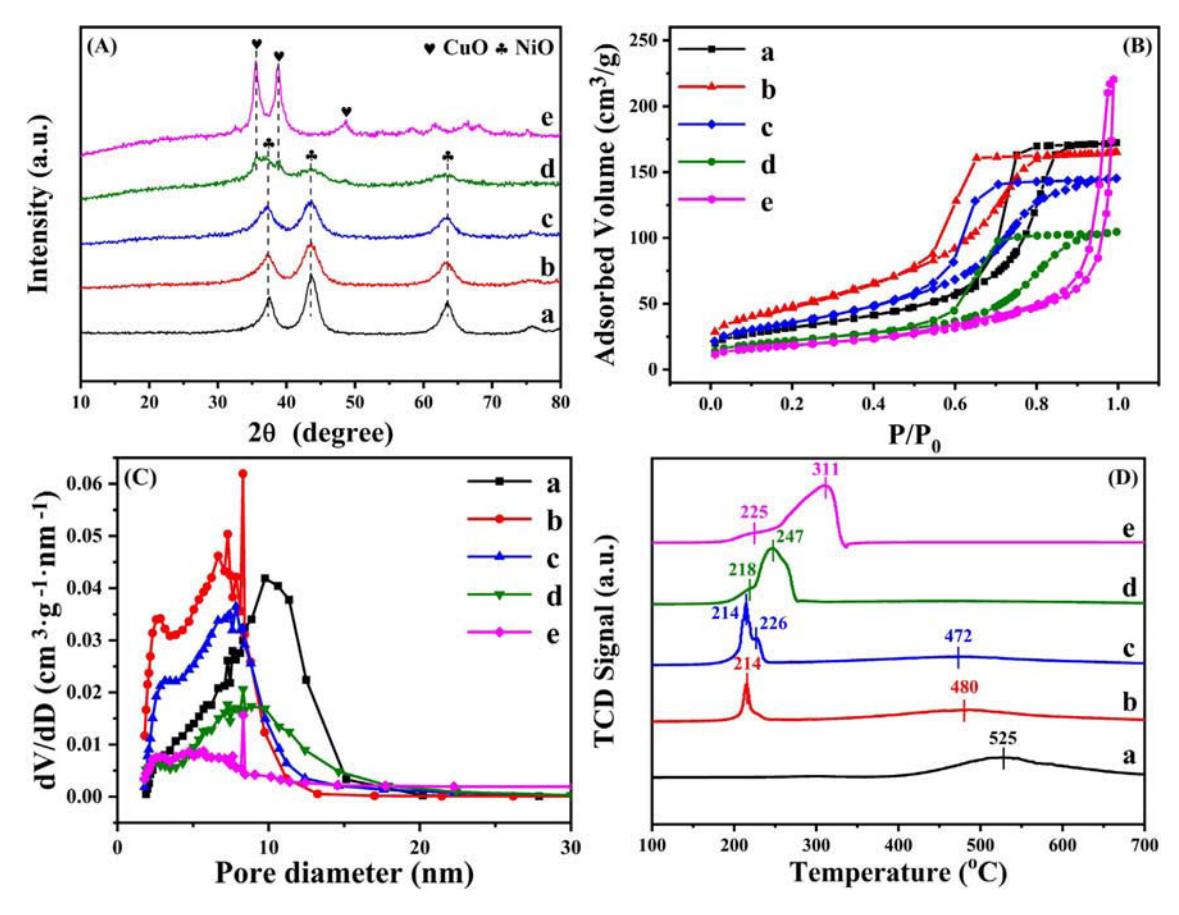
The extent of reduction was also calculated from the data in Fig. 1D by performing a peak fitting and integration; the results are reported in Fig. S3 and Table S2; the peaks for highly dispersed CuO species, CuO clusters of different sizes, and CuO species with various crystallinities were denoted as  $\alpha$ ,  $\beta$ - $\delta$  and  $\epsilon$ - $\theta$ , respectively. In general, the total  $H_2$  consumption increases with increasing copper content, but the nature of the species being reduced evolves as the Ni-to-Cu ratio varies. Given that the higher the reduction peak temperature the larger the particle size, it can be concluded that the CuO species are highly dispersed and have small size clusters in the Cu $_{0.5}$ Ni $_{2.5}$ AlO $_{y}$  and Cu $_{1}$ Ni $_{2}$ AlO $_{y}$  catalysts but form larger clusters with different particle sizes in the Cu $_{2}$ Ni $_{1}$ AlO $_{y}$  catalyst. Moreover, in the Cu $_{3}$ AlO $_{y}$  catalyst, the majority of the copper is in the form of crystallized CuO species; its reduction temperature is the highest, and it is the most difficult sample to reduce.

**Table 1** Physical properties and catalytic activity of the  $Cu_xNi_{3-x}AlO_y$  catalysts.

Entry	Catalysts	$S_{BET} (m^2/g)$	Actual atom ratio (Cu/Ni/Al) d	Conversion (%) e	Selectivity (%) <sup>e</sup>	Yield (%) <sup>f</sup>	TOF (h <sup>-1</sup> )
1	Cu <sub>3</sub> AlO <sub>v</sub> <sup>a</sup>	66	3.10/0/1	31	7.8	2.4	1.1
2	Cu <sub>2</sub> Ni <sub>1</sub> AlO <sub>v</sub> <sup>a</sup>	79	1.94/0.94/1	90	82	74	14
3	Cu <sub>1</sub> Ni <sub>2</sub> AlO <sub>v</sub> <sup>a</sup>	128	1.00/1.89/1	60	88	53	8.2
4	Cu <sub>0.5</sub> Ni <sub>2.5</sub> AlO <sub>v</sub> <sup>a</sup>	175	0.50/2.28/1	34	54	18	5.0
5	Ni <sub>3</sub> AlO <sub>v</sub> <sup>a</sup>	115	0/2.76/1	25	3.4	0.85	_
6	Cu <sub>2</sub> Ni <sub>1</sub> AlO <sub>v</sub> <sup>b</sup>	79	1.94/0.94/1	9.6	8.3	0.80	0.20
7	Cu <sub>2</sub> Ni <sub>1</sub> AlO <sub>y</sub> <sup>c</sup>	79	1.94/0.94/1	98	99	97	18

Reaction conditions: FAL (0.2525 g), catalyst (50 mg), isopropanol (15 mL), 1.5 h.

- <sup>a</sup> H<sub>2</sub> (1.4 MPa), 110 °C.
- <sup>b</sup> N<sub>2</sub> (1.6 MPa), 120 °C.
- <sup>c</sup> H<sub>2</sub> (1.6 MPa), 120 °C.
- <sup>d</sup> Actual bulk atom ratio of Cu/Ni/Al was measured by ICP-OES.
- <sup>e</sup> Experimental error < ± 5%.
- f Yield = Conversion of FAL × Selectivity of FOL.



 $\textbf{Fig. 1.} \ \, (A) \ \, \textbf{XRD} \ \, \textbf{patterns,} \ \, (B) \ \, N_2 \ \, \textbf{adsorption-desorption isotherms,} \ \, (C) \ \, \textbf{Pore size distribution and} \ \, (D) \ \, \textbf{H}_2 - \textbf{TPR} \ \, \textbf{profiles obtained with the} \ \, \textbf{Cu}_x \textbf{Ni}_{3-x} \textbf{AlO}_y \ \, \textbf{catalysts} \ \, (a: \textbf{Ni}_3 \textbf{AlO}_y, \ \, \textbf{b:} \ \, \textbf{Cu}_{0.5} \textbf{Ni}_{2.5} \textbf{AlO}_y, \ \, \textbf{c:} \ \, \textbf{Cu}_1 \textbf{Ni}_2 \textbf{AlO}_y, \ \, \textbf{e:} \ \, \textbf{Cu}_2 \textbf{Ni}_1 \textbf{AlO}_y, \ \, \textbf{e:} \ \, \textbf{Cu}_3 \textbf{AlO}_y).$ 

#### 3.3. Catalytic hydrogenation performance

# 3.3.1. Catalytic activity over $Cu_xNi_{3-x}AlO_v$

Next, we examined the catalytic activity of the  $Cu_xNi_{3-x}AlO_y$  catalysts. A summary of the results is provided in Table 1, in the form of total conversion and selectivity toward FOL production after 1.5 h at 110 °C and under a  $H_2$  pressure of 1.4 MPa (additional conditions are indicated in the footnotes of Table 1). Some conversion was seen with the  $Cu_3AlO_y$  and  $Ni_3AlO_y$  catalysts, but significantly better performance was obtained with the  $Cu_xNi_{3-x}AlO_y$  samples. As listed in Table S1, we replaced  $H_2$  by  $N_2$  to investigate the catalytic performance of the  $Ni_3AlO_y$  and  $Cu_3AlO_y$  catalysts

under the same conditions above. The results showed similar activity regardless of either in  $H_2$  or  $N_2$  atmosphere over the  $Ni_3AlO_y$  catalyst. Therefore, we believe that what happens on the surface of the  $Ni_3AlO_y$  catalyst is a hydrogen transfer reaction [34,35]. It can be seen from Table S1 that the activity of the  $Cu_3AlO_y$  catalyst under  $N_2$  atmosphere is significantly lower than that of the reaction in  $H_2$ , and there is no formation of FOL. This indicates that the hydrogenation reaction mainly occurs rather than the hydrogen transfer reaction on the  $Cu_3AlO_y$  catalyst. In addition, higher activity and selectivity were observed as the Ni content was decreased, with the  $Cu_2Ni_1AlO_y$  catalyst exhibiting the best catalytic activity: a 90% FAL conversion of FAL with 82% FOL selectiv-

ity was measured in that case. A slightly better selectivity was obtained with  $\text{Cu}_1\text{Ni}_2\text{AlO}_y$ , but the difference is not large, and comes at the expense of a decrease in total activity. We also tested the conversion to FAL and distribution of FOL with reaction time over the  $\text{Cu}_x\text{Ni}_{3-x}\text{AlO}_y$  catalysts. As shown in Fig. S4, we can find that the conversion and selectivity of all the catalysts in the first hour are relatively low, and the conversion of FAL and selectivity of FOL increase sharply with reaction time after 1 h over all the  $\text{Cu}_x\text{Ni}_{3-x}\text{AlO}_y$  catalysts. In addition, we performed the reactions by using benzene to replace isopropanol under  $\text{N}_2$  over  $\text{Ni}_3\text{AlO}_y$  and  $\text{Cu}_3\text{AlO}_y$ , respectively. It is observed that nearly 11% conversion to FAL is obtained without formation of FOL, and the color of solution becomes dark. So, we think FAL may be polymerization itself under the such reaction conditions of high pressure and temperature.

On the basis of the conversion data in Table 1 and the Cu dispersion information available from the characterization of the  $\text{Cu}_x\text{Ni}_{3-x}\text{AlO}_y$  catalysts, initial TOF values were estimated for the FAL hydrogenation reaction (Table 1, last column). The TOFs are ordered, from high to low, following the  $\text{Cu}_2\text{Ni}_1\text{AlO}_y$  (14  $h^{-1}$ ) >  $\text{Cu}_1\text{-Ni}_2\text{AlO}_y$  (8.2  $h^{-1}$ ) >  $\text{Cu}_{0.5}\text{Ni}_{2.5}\text{AlO}_y$  (5.0  $h^{-1}$ ) >  $\text{Cu}_3\text{AlO}_y$  (1.1  $h^{-1}$ ), it can be seen that the TOF value of the  $\text{Cu}_2\text{Ni}_1\text{AlO}_y$  catalyst is 12.7 times higher than that of the  $\text{Cu}_3\text{AlO}_y$  sample, an observation that points to the beneficial effect of the added Ni in the mixed-oxide samples. The mixed oxide catalysts perform much better in terms to the weight of the catalyst used as well: the reaction rate over  $\text{Cu}_2\text{Ni}_1\text{AlO}_y$  (32 mmol·g $^-\text{h}^-\text{1}$ ) is 2.9 times higher than that over  $\text{Cu}_3\text{AlO}_y$  (11 mmol·g $^-\text{h}^-\text{1}$ ).

#### 3.3.2. Effect of reaction conditions over Cu<sub>2</sub>Ni<sub>1</sub>AlO<sub>v</sub>

We also investigated the effects of reaction temperature, reaction time, and  $\rm H_2$  pressure on activity over the  $\rm Cu_2Ni_1AlO_y$  catalyst. As expected, the conversion of FAL increases gradually with increasing reaction temperature from 80 °C to 120 °C, but, interestingly, so does the selectivity toward FOL production (Fig. 2A); only after reaching 140 °C did both activity and selectivity started to decrease, possibly because of catalyst poisoning from reactant decomposition. Similar trends were seen at a fixed set temperature as a function of either reaction time (Fig. 2B) or  $\rm H_2$  pressure (Fig. 2C).

# 3.3.3. Reusability of Cu<sub>2</sub>Ni<sub>1</sub>AlO<sub>y</sub>

The reusability of the  $Cu_2Ni_1AlO_y$  catalyst for FAL hydrogenation was briefly tested. After every run, the catalyst was washed with isopropanol and water to remove the organics adsorbed on the surface of catalyst, and dried overnight in a vacuum oven. Fig. 2D shows how the  $Cu_2Ni_1AlO_y$  catalyst retains most of its activity and selectivity after three runs.

#### 3.4. Characterization of the catalysts after reaction

# 3.4.1. Reaction under $N_2$ atmosphere

To test that the hydrogen atoms in the FAL hydrogenation come from  $H_2$  and not via a hydrogen transfer reaction from isopropanol (the solvent) [28], a reaction was run under a  $N_2$  atmosphere: virtually no activity was detected in that case (Table 1, Entry 6), confirming that this is a  $H_2$  driven reaction.

# 3.4.2. XRD patterns after reaction

The  $\text{Cu}_2\text{Ni}_1\text{AlO}_y$  catalyst was also characterized by XRD after treatment under different conditions, including by imitating the activity tests but without the addition of FAL. As shown in Fig. 3A, exposure to a mixture of  $\text{N}_2$  + isopropanol leads to virtually no changes in the structure of the fresh catalyst: neither  $\text{N}_2$  nor isopropanol are capable of reducing the CuO species to  $\text{Cu}^0$ . In another experiment, isopropanol was replaced with xylene, a non-reducing

and high-boiling-point (>120 °C) solvent that is also inert in the presence of H<sub>2</sub>: the crystalline structure of the Cu<sub>2</sub>Ni<sub>1</sub>AlO<sub>y</sub> catalysts is basically the same after exposures to the H<sub>2</sub> atmosphere in both solvents: the characteristic diffraction peaks at  $2\theta$  = 35.5 and 38.8° seen with the fresh sample, corresponding to CuO (PDF JCPDS 89-5899), are replaced by new features at  $2\theta$  = 43.5, 50.5 and 74.1°, which are associated to Cu<sup>0</sup> (PDF JCPDS 89-2838). On the other hand, the characteristic diffraction peak at  $2\theta$  = 37.5° attributed to NiO (PDF JCPDS 75-0197) is still observed. This indicates that, regardless of the nature of the solvent (isopropanol or xylene), the CuO species can be reduced to Cu<sup>0</sup> in situ at 120 °C under a 1.6 MPa H<sub>2</sub> atmosphere in 1.5 h. All these results confirm that, in addition to serving as the hydrogen donor for FAL hydrogenation, H<sub>2</sub> also acts as a reducing agent for the CuO species.

All the five samples were also characterized by XRD after reaction. The results are shown in Fig. 3B, with the once-used Cu<sub>x</sub>Ni<sub>3-x</sub>- $AlO_v$  catalysts denoted as  $Cu_xNi_{3-x}AlO_y$ -1. The spectra from Cu<sub>0.5</sub>Ni<sub>2.5</sub>AlO<sub>v</sub>-1 and Cu<sub>1</sub>Ni<sub>2</sub>AlO<sub>v</sub>-1 display mainly the characteristic diffraction peaks of NiO; those from Cu phases are not discernible, perhaps because of the low amount of CuO in these catalysts, and/or because any reduced Cu<sup>0</sup> species may be highly dispersed on the surface of the catalyst (a conclusion confirmed by XPS and AES below). This result also reiterates the fact that NiO cannot be reduced in situ under the reaction condition. With Cu<sub>2</sub>Ni<sub>1</sub>AlO<sub>v</sub>-1, similar peaks to those observed with the previous samples are detected, but they are weaker and broader. It appears that in this case there is less crystallinity, and much of the NiO phase is in the form of small crystallites (no CuO-containing crystallites are seen). Complementary H2-TPR data obtained for this catalyst after having used it once (Cu<sub>2</sub>Ni<sub>1</sub>AlO<sub>v</sub>-1) show a reduction peak at 214 °C (Fig. S5), demonstrating that the dispersed CuO species in Cu<sub>2</sub>Ni<sub>1</sub>AlO<sub>v</sub> are only partially reduced after reaction, although the low value of this temperature also indicates that the unreduced CuO species are re-dispersed on the catalyst surface during reaction. We conclude that, under reaction conditions (110 °C, 1.4 MPa  $H_2$ , 1.5 h), any CuO clusters (the peaks at  $\leq$  250 °C, see H<sub>2</sub>-TPR in Fig. S3) can be reduced at least in part in situ during reaction, but that the large CuO crystallites (>265 °C in the H<sub>2</sub>-TPR in Fig. S3) cannot. Finally, in the case of Cu<sub>3</sub>-AlO<sub>v</sub>, no obvious changes are seen after versus before catalysis: the copper species still remain in the form of CuO. An important conclusion from these observations is that the NiO phase appears to aid in the copper reduction process.

# 3.4.3. XPS of catalysts after reaction

XPS characterization of our Cu<sub>x</sub>Ni<sub>3-x</sub>AlO<sub>v</sub> catalysts used once (Cu<sub>x</sub>Ni<sub>3-x</sub>AlO<sub>v</sub>-1) was carried out as well (Fig. 4A). The traces in the 930-937.5 eV binding energy (BE) XPS region, which correspond to Cu 2p<sub>3/2</sub> photoelectrons [36], were fitted to two characteristic peaks, of which the feature at BE = 932.0 eV comes from the low oxidation state species (Cu<sup>0</sup> and/or Cu<sup>+</sup>) [37], and the one at BE = 934.5 eV is assigned to the  $Cu^{2+}$  species [36]. In addition, the satellite peak seen at BE = 942.5 eV also belongs to Cu<sup>2+</sup> species [38,39]. Spectra for the Cu LMM AES were also acquired to carry out a more definitive oxidation state assignment (Fig. 4B). Two peaks were again extracted by peak fitting from the traces in the of 905-925 eV kinetic energy (KE) range, characteristic of  $Cu^{0}$  (KE = 917.6 eV) and  $Cu^{+}$  (KE = 913.8 eV) species [40]. The detection of significant intensities for the Cu<sup>0</sup> and Cu<sup>+</sup> species clearly indicates that the original CuO species on the surface of these catalysts are reduced in situ to low-oxidation-state copper species during reaction. Further quantitative analysis of the intensities of all these XPS and AES features, summarized in Table 2, shows that much of the copper in the used mixed-oxide samples is in fact in metallic state, and that both the absolute coverages and the fractions of Cu in zero and +1 oxidation states (relative

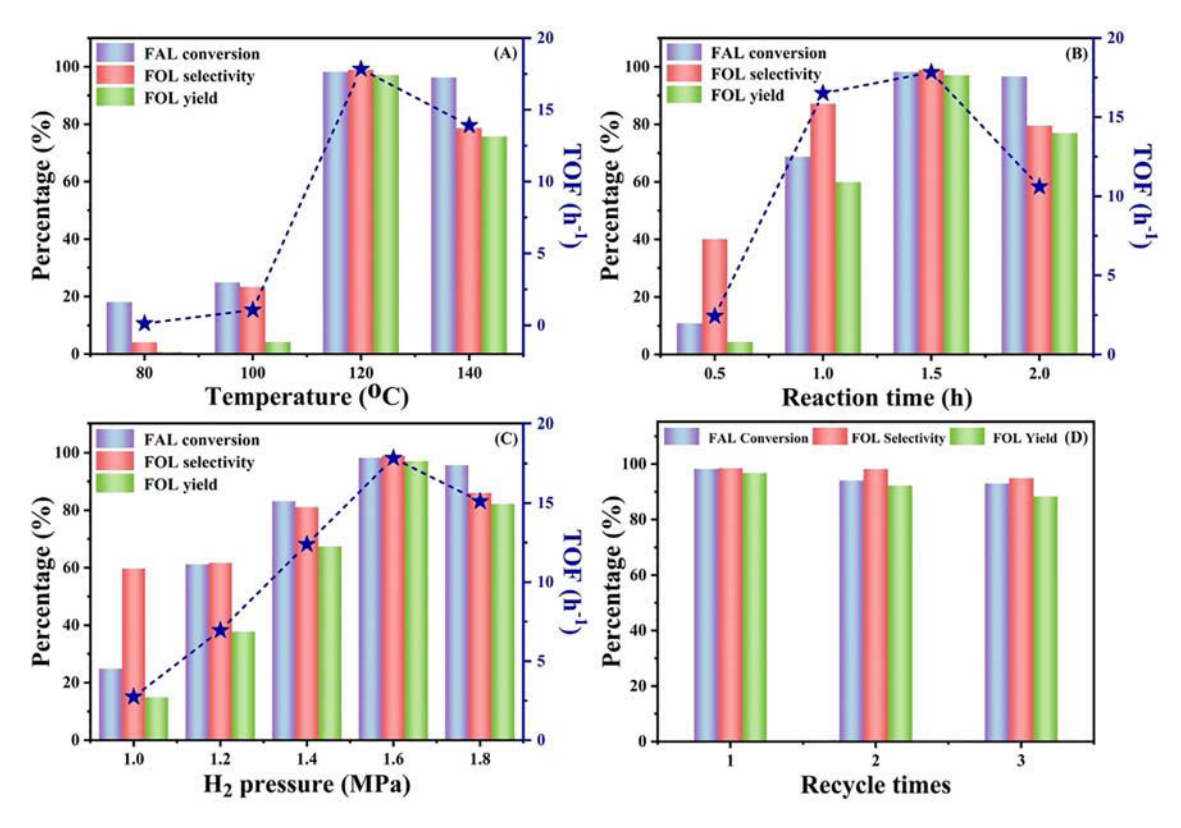
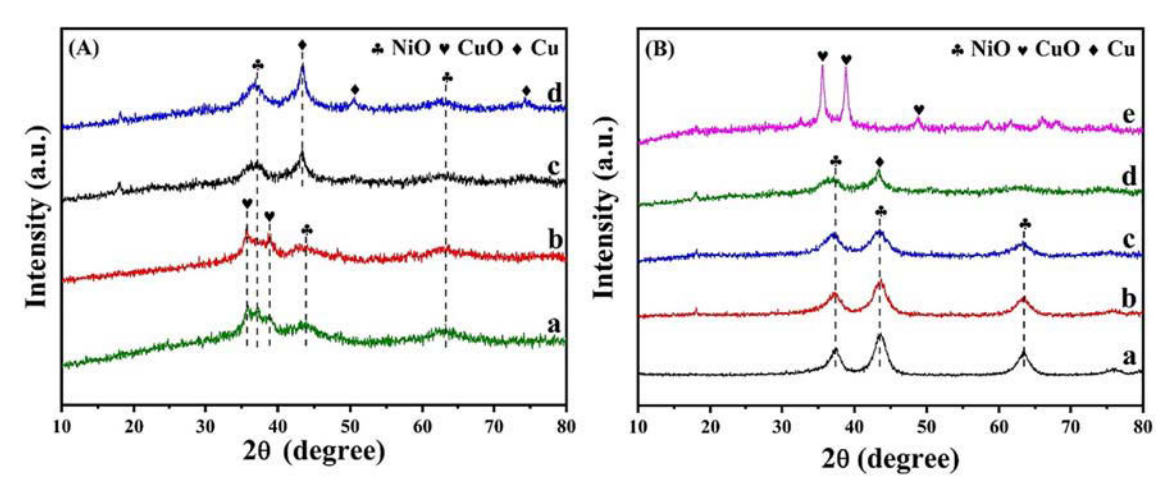


Fig. 2. The effect of reaction conditions on activity and reusability of the  $Cu_2Ni_1AlO_y$  catalyst (Reaction conditions: 0.2525 g FAL, 50 mg catalyst, 15 mL isopropanol, (A) 1.6 MPa  $H_2$ , 1.5 h; (B) 120 °C, 1.6 MPa  $H_2$ ; (C) 120 °C, 1.5 h; (D) 120 °C, 1.6 MPa  $H_2$ , 1.5 h).



**Fig. 3.** (A) XRD patterns of the  $Cu_2Ni_1AlO_y$  catalyst after different treatments: a: fresh catalyst; b:  $N_2$  + isopropanol; c:  $H_2$  + isopropanol; d:  $H_2$  + xylene (Treatment conditions: 50 mg catalyst, 120 °C, 1.6 MPa  $N_2/H_2$ , 1.5 h, 15 mL of isopropanol/xylene). (B) XRD patterns of the catalysts used once: a:  $Ni_3AlO_y$ -1, b:  $Cu_{0.5}Ni_{2.5}AlO_y$ -1, c:  $Cu_1Ni_2AlO_y$ -1, d:  $Cu_2Ni_1AlO_y$ -1, e:  $Cu_3AlO_y$ -1 (Reaction conditions: 0.2525 g FAL, 50 mg catalyst, 15 mL isopropanol, 110 °C, 1.4 MPa  $H_2$ , 1.5 h).

to the total amount of Cu) increase with decreasing Ni content (the latter trend being less pronounced); the  $\text{Cu}_2\text{Ni}_1\text{AlO}_y$ -1 sample has the most surface  $\text{Cu}^0$  species among these catalysts. With the  $\text{Cu}_3$ -AlO $_y$ -1 catalyst, however, a much smaller fraction of the CuO species can be reduced to  $\text{Cu}^0$  species in situ during the reaction. We speculate that this may be due to the higher crystallinity of the CuO species and the larger particle size in the Cu-only solid, as confirmed by the XRD results (Fig. 3B); such large CuO crystallites are difficult to reduce in situ, a conclusion also consistent with the H<sub>2</sub>-TPR results (Fig. 1D). It is important to highlight that one role of the

NiO component in our catalyst is to help keep the initial CuO domains small, aiding in this way with their reduction. It may be that NiO also aids with  $H_2$  dissociation, as reported in other contexts [41], and therefore with the copper oxide reduction as well as with FAL hydrogenation steps.

Cu<sup>0</sup> species have been reported to facilitate the formation of FOL from FAL hydrogenation by favoring adsorption via the oxygen atoms [42–44]. With this in mind, in Fig. 4C we have plotted the conversion of FAL against the amount of Cu<sup>0</sup> on the catalyst surface in search of any meaningful correlation. It can be seen in that figure

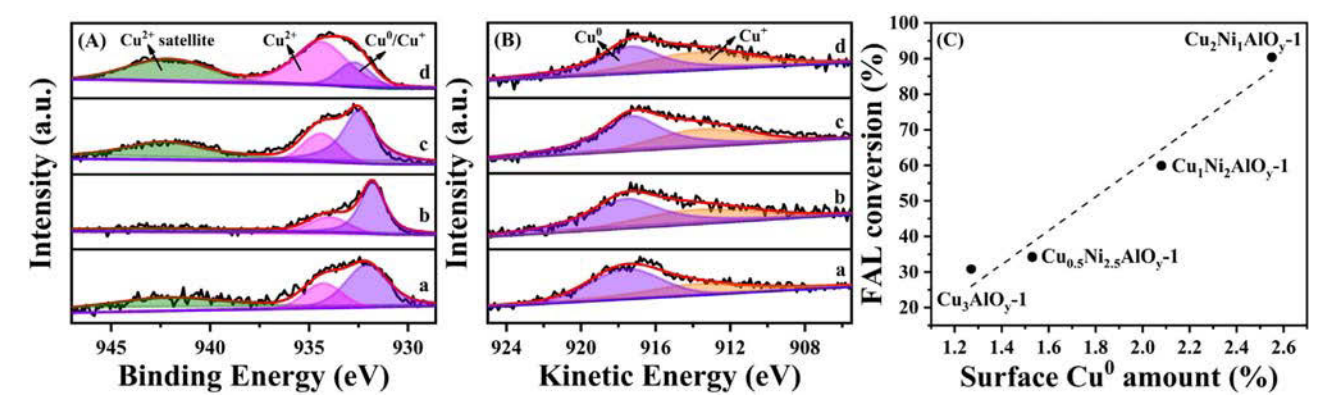


Fig. 4. (A) Cu  $2p_{3/2}$  XPS, (B) Cu LMM AES and (C) Relationship between  $Cu^0$  surface coverage and FAL conversion with the  $Cu_xNi_{3-x}AlO_y$ -1 catalysts (a:  $Cu_{0.5}Ni_{2.5}AlO_y$ -1, b:  $Cu_1Ni_2AlO_y$ -1, c:  $Cu_2Ni_1AlO_y$ -1, d:  $Cu_3AlO_y$ -1).

**Table 2** Surface elemental composition of the  $Cu_xNi_{3-x}AlO_y$  catalysts after being used once for catalysis.

Samples	Surface composition (at%)				(Cu <sup>0</sup> + Cu <sup>+</sup> )/Cu (%) <sup>a</sup>	Cu <sup>0</sup> /(Cu <sup>0</sup> + Cu <sup>+</sup> ) (%) b	Surface Cu <sup>0</sup> coverage (%)	
	Cu	Ni	Al	0				
Cu <sub>0.5</sub> Ni <sub>2.5</sub> AlO <sub>v</sub> -1	3.66	25.61	16.66	54.07	69.8	60.0	1.53	
Cu <sub>1</sub> Ni <sub>2</sub> AlO <sub>v</sub> -1	4.36	16.92	25.87	52.85	74.0	64.5	2.08	
Cu <sub>2</sub> Ni <sub>1</sub> AlO <sub>v</sub> -1	5.32	8.92	33.59	52.17	71.4	67.1	2.55	
Cu <sub>3</sub> AlO <sub>v</sub> -1	10.44	_	44.98	44.58	23.5	51.5	1.27	

<sup>&</sup>lt;sup>a</sup> (Cu<sup>0</sup> + Cu<sup>+</sup>)/Cu surface atom ratio calculated from the XPS data.

that, indeed, there is a close linear relationship between the two parameters, with the extent of FAL conversion increasing with the amount of Cu<sup>0</sup> atoms exposed. This corroborates that the Cu<sup>0</sup> species on the surface of the catalyst may play a central role in the hydrogenation of FAL. We also investigated the effects of the surface Cu<sup>+</sup> species on the catalytic activity of the Cu<sub>x</sub>Ni<sub>3-x</sub>AlO<sub>y</sub> catalysts, and the results are shown in Fig. S6A. The Cu<sup>+</sup> species on the catalyst surface is positively correlated with the FAL conversion, which indicates that the Cu<sup>+</sup> species may be beneficial to the FAL hydrogenation reaction.

As shown in Fig. S2B and S7, we can find that the binding energy and peak shape of the NiO species on the used  $Cu_xNi_{3-x}AlO_y$  catalysts do not change significantly compared with the fresh  $Cu_x-Ni_{3-x}AlO_y$  catalysts (Fig. S2B). In addition, no signal for  $Ni^0$  (BE = 852.5 eV) [45,46] was detected in any of the catalysts used in this study; clearly, the NiO species in these catalysts cannot be reduced in situ during reaction. Moreover, the amount of NiO species on the surface of the  $Cu_xNi_{3-x}AlO_y-1$  catalysts is negatively correlated with the conversion of FAL (Fig. S6B), so surface NiO species does not directly contribute to the catalytic activity.

#### 3.4.4. TEM images of catalyst after reaction

The structure of the Cu<sub>2</sub>Ni<sub>1</sub>AlO<sub>y</sub> catalyst used once (Cu<sub>2</sub>Ni<sub>1</sub>AlO<sub>y</sub>-1) was further characterized by electron microscopy. The TEM (Fig. 5A) and high-resolution TEM (HRTEM) (Fig. 5B) images show typical NPs with lattice distances of 0.21 and 0.24 nm, corresponding to the (111) planes of Cu and NiO, respectively. Furthermore, the selected area electron diffraction (SAED) pattern in Fig. 5C show three regular diffraction rings assigned to the (111) crystal plane of NiO (2 $\theta$  = 37.5°), the (111) crystal plane of Cu (2 $\theta$  = 43.5°), and the (220) crystal plane of NiO (2 $\theta$  = 63.5°); these results are consistent with the XRD results (Fig. 3A). High-angle annular dark-field scanning TEM (HAADF-STEM) imaging (Fig. 5D) and energy dispersive X-ray spectroscopy (EDS) mapping

(Fig. 5E-H) also reveal the homogeneous distribution of the elements (Cu, Ni, Al, and O) in the  $\text{Cu}_2\text{Ni}_1\text{AlO}_y$ -1 catalyst; the two Cu and Ni phases seem to be well intermixed, an arrangement beneficial for the promotion of the FAL hydrogenation.

#### 3.4.5. In situ FT-IR spectra of FAL adsorption

In situ FT-IR spectroscopy was used to determine the adsorption mode of FAL on the surfaces of our catalysts (Fig. 6). In all cases, strong peaks are seen in the 1600-1720 cm<sup>-1</sup> region associated with C = O stretching modes in FAL [47-49]. With the fresh  $Cu_3$ -AlO<sub>v</sub>, Cu<sub>2</sub>Ni<sub>1</sub>AlO<sub>v</sub>, and Ni<sub>3</sub>AlO<sub>v</sub> catalysts (Fig. 6A), the main feature is centered at 1670, 1664, and 1673 + 1679  $\text{cm}^{-1}$ , respectively, and all the spectra show a second blue-shifted feature at 1693 cm<sup>-1</sup>. Once the catalysts are used, their capacity for adsorption decreases, and consequently the intensity of the adsorbed FAL IR peaks decreases in absolute terms (notice the change of scale in Fig. 6B). We think that the redispersion of the Cu<sup>0</sup> species obtained by in-situ reduction on the surface of the catalyst, covering NiO and other species, which leads to a decrease in the adsorption capacity to FAL derived from NiO of the Cu<sub>2</sub>Ni<sub>1</sub>AlO<sub>v</sub> catalyst. Nevertheless, some FAL uptake is still detected, manifested by the same strong band at 1670 cm<sup>-1</sup> and the second weaker one at  $1695~\text{cm}^{-1}$  with both  $\text{Cu}_2\text{Ni}_1\text{AlO}_\text{v}\text{-1}$  and  $\text{Cu}_3\text{AlO}_\text{v}\text{-1}$  catalysts. The similarity of the spectra obtained with the two used catalysts, and the significant differences seen between those and the one recorded with fresh  $Ni_3AlO_v$  (in which the C = O main peak is split and blue-shifted, and where the 1693 cm<sup>-1</sup> feature is much more intense in relative terms, compared with the main peaks), suggests adsorption on the Cu phase. Moreover, the frequency values and relative intensities reported in Fig. 6 indicate an adsorption geometry on Cu<sup>0</sup> with the carbonyl bond oriented perpendicular to the surface, likely via the oxygen atom; this adsorption geometry is typical of oxygenates on coinage metals, as reported before, and is what justifies the high selectivity exhibited by Cu surface toward

<sup>&</sup>lt;sup>b</sup>  $Cu^0/(Cu^0 + Cu^+)$  surface atom ratio calculated from the AES data.

<sup>&</sup>lt;sup>c</sup> Surface  $Cu^0$  coverage = Cu surface composition  $\times [(Cu^0 + Cu^+)/Cu] \times [Cu^0/(Cu^0 + Cu^+)]$ .

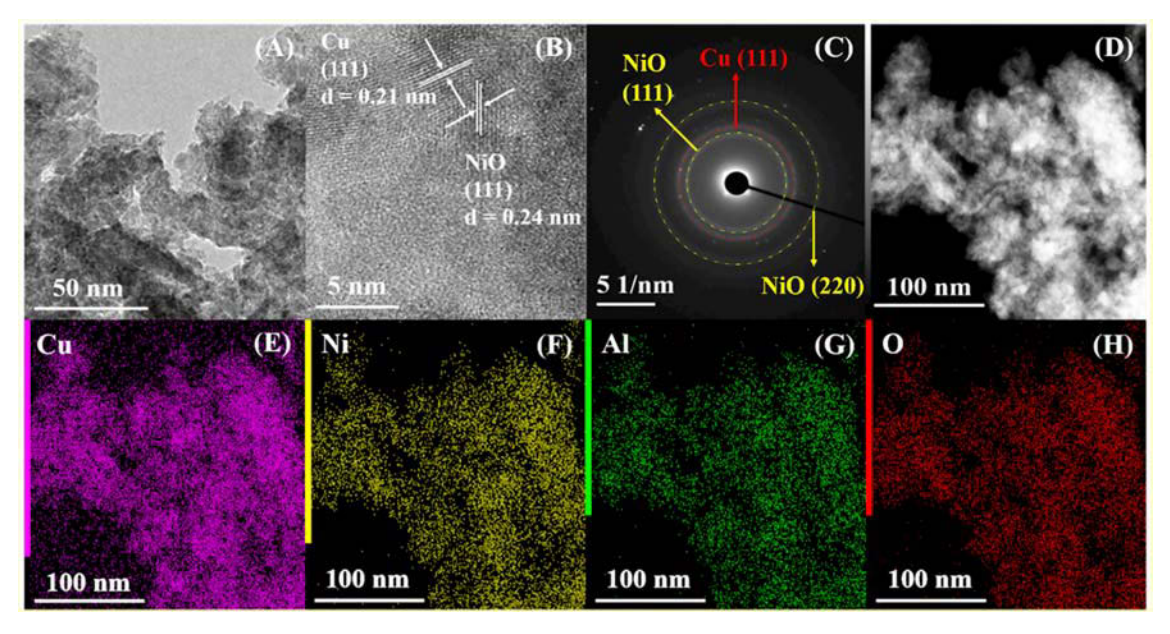


Fig. 5. TEM image (A), HRTEM image (B), SAED pattern (C), HAADF-STEM image (D), EDS mapping of Cu (E), Ni (F), Al (G) and O (H) of the Cu<sub>2</sub>Ni<sub>1</sub>AlO<sub>V</sub>-1 catalyst.

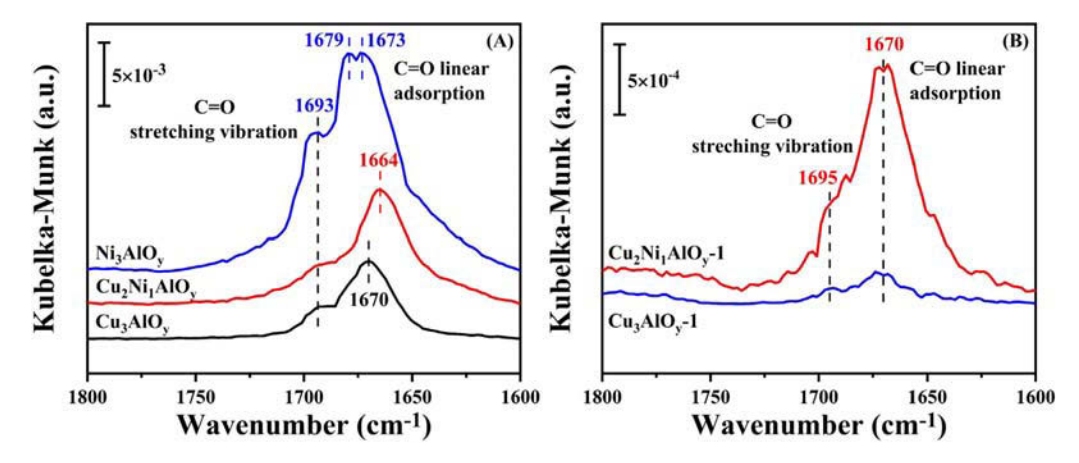


Fig. 6. In situ FT-IR spectra of FAL adsorption on (A) fresh Cu<sub>3</sub>AlO<sub>y</sub>, Cu<sub>2</sub>Ni<sub>1</sub>AlO<sub>y</sub>, and Ni<sub>3</sub>AlO<sub>y</sub>; and (B) used Cu<sub>3</sub>AlO<sub>y</sub>-1 and Cu<sub>2</sub>Ni<sub>1</sub>AlO<sub>y</sub>-1, after flowing FAL for 60 min at 25 °C.

hydrogenation at the carbonyl group [50–54]. The peaks are much more intense on  $\text{Cu}_2\text{Ni}_1\text{AlO}_y$ -1 than on  $\text{Cu}_3\text{AlO}_y$ -1, but that difference is easily explained by the larger amount of  $\text{Cu}^0$  atoms exposed in the former case, as indicated by the XPS/AES data in Table 2. It may be that this high FAL adsorption capacity is one of the reasons that make  $\text{Cu}_2\text{Ni}_1\text{AlO}_y$ -1 such an active catalyst for its hydrogenation. Therefore, we think the main adsorption sites is the  $\text{Cu}^0$  species obtained by in-situ reduction on the  $\text{Cu}_2\text{Ni}_1\text{AlO}_y$ -1 catalyst surface instead of the NiO or other species.

On the basis of the results from all of these post-catalysis characterization experiments, the different activity seen with the various  $\text{Cu}_x\text{Ni}_{3-x}\text{AlO}_y$  catalysts can be explained mainly by the differences in the amount of CuO species on the catalyst reduced to Cu^0 in situ during reaction. As indicated by the H2-TPR data in Fig. S3, the Cu species associated with the three  $\alpha, \, \beta,$  and  $\gamma$  peaks can be fully reduced at relatively low temperature, and even the oxide associated with peak  $\delta$  can be partially reduced by H2 in situ during the reaction process. Moreover, the interaction between CuO and NiO appears to enhance the dispersion of the copper species on the catalyst, and with that reduce the crystallinity and particle size of the CuO species. This lower cryst

tallinity and smaller particle size make the CuO species on the catalyst surface easier to reduce in situ under reaction conditions. The data from the isothermal adsorption-desorption experiments further indicate that the addition of nickel increases the specific surface area of the catalysts, and a larger specific surface area is also conducive to a higher dispersion of the Cu species. All of these effects are maximized in the Cu<sub>2</sub>Ni<sub>1</sub>AlO<sub>v</sub>-1 catalyst, which exhibits the largest surface coverage of metallic copper, and consequently the highest activity and selectivity for FAL hydrogenation. A quantitation of the amount of Cu<sup>0</sup> species exposed on the surface and available for catalysis, afforded by the XPS experiments (Table 2), make the connection between Cu<sup>0</sup> site availability and catalytic performance more evident and quantitative, and, moreover, the FT-IR results (Fig. 6) directly prove that the FAL adsorption occurs mainly on the surface of Cu<sup>0</sup> species. The relationship between reaction time and product distribution (Fig. S4) can also confirm this conclusion. We believe that the amount of Cu<sup>0</sup> species obtained by in-situ reduction of the CuO species on the catalyst surface should gradually increase with the reaction time. Thus, the FOL selectivity is low due to less amount of Cu<sup>0</sup> species formed, and the polymerization of furfural should be primary over the surface of catalyst with metal oxidation state in 1 h. When enough  $\text{Cu}^0$  species obtained by in-situ reduction, the FAL hydrogenation reaction is dominant, increasing the conversion of FAL and selectivity of FOL quickly. It is also found that the catalytic activity for FAL hydrogenation is linearly correlated to the content of  $\text{Cu}^0$  species on the catalyst surface (Fig. 4C). Furthermore, the difference in the selectivity to FOL over the  $\text{Cu}_x \text{Ni}_{3-x} \text{AlO}_y$  catalysts is directly related to the amount of their surface  $\text{Cu}^0$  species. In other words, the content of  $\text{Cu}^0$  species on the catalyst surface is positively correlated with the selectivity of FOL. The main role of the added NiO is to facilitate Cu dispersion and reducibility, and maybe also to help with  $\text{H}_2$  activation during catalysis.

As for the effect of reaction conditions on the catalytic performance over the  $\text{Cu}_2\text{Ni}_1\text{AlO}_y$  catalyst, the data in Fig. 2 indicates that the CuO surface species cannot be effectively reduced at low reaction temperature or low  $\text{H}_2$  pressure; in-situ reduction of the CuO phase to create the  $\text{Cu}^0$  sites responsible for the promotion of hydrogenation catalysis requires specific minimum temperature and pressure reaction conditions. It can be said that, in general, hydrogenations with Cu-based catalysts are limited by the difficulty to reduce CuO to  $\text{Cu}^0$  species, more so with larger and crystalline metal oxide nanoparticles. Thanks to the increased Cu-phase dispersion achieved here by adding NiO to our mixed-oxide catalysts, that reduction is facilitated, and thus hydrogenation catalysis can be carried out more efficiently and under milder (low temperature) conditions.

#### 4. Conclusions

In summary, a series of Cu<sub>x</sub>Ni<sub>3-x</sub>AlO<sub>y</sub> mixed-oxide catalysts was designed and prepared by using CuxNi3-xAl-LDH hydrotalcites as precursors, and employed to promote the selective hydrogenation of FAL to FOL. The Cu<sub>2</sub>Ni<sub>1</sub>AlO<sub>y</sub> catalyst was found to exhibit the best catalytic total activity as well as a high selectivity toward the production of FOL, a behavior that can be ascribed to the in situ formation of a large coverage of Cu<sup>0</sup> species on the catalyst during the catalytic reaction. By combining results from a variety of catalyst characterization experiments, it was determined that higher surface Cu<sup>0</sup> content results in a higher uptake of FAL, which in turns leads to higher catalytic activity. As a result, the reaction rate measured with the Cu<sub>2</sub>Ni<sub>1</sub>AlO<sub>v</sub> catalyst was 2.9 times larger than that obtained with the Cu-only Cu<sub>3</sub>AlO<sub>v</sub> catalyst, and the TOF value was 12.7 times larger. Compared with other catalysts made with traditional non-precious metals, the advantage of our samples is that they can be used without any pre-reduction treatment; that speeds up the reaction process and saves energy. In addition, our Cu2Ni1AlOv catalyst operates selectively and efficiently under relatively mild reaction conditions.

#### **Declaration of Competing Interest**

The authors declare that they have no known competing financial interests or personal relationships that could have appeared to influence the work reported in this paper.

# Acknowledgements

This project was supported by the National Natural Science Foundation of China (22076040) and Heilongjiang Provincial Natural Science Foundation of China (LH2020B021). Financial support for FZ was provided by the US National Science Foundation, Division of Chemistry, Grant No. NSF-CHE1953843.

#### Appendix A. Supplementary material

Supplementary data to this article can be found online at https://doi.org/10.1016/j.jcat.2021.10.009.

#### References

- [1] W. Gao, S. Liang, R. Wang, Q. Jiang, Y. Zhang, Q. Zheng, B. Xie, C.Y. Toe, X. Zhu, J. Wang, L. Huang, Y. Gao, Z. Wang, C. Jo, Q. Wang, L. Wang, Y. Liu, B. Louis, J. Scott, A.-C. Roger, R. Amal, H. He, S.-E. Park, Industrial carbon dioxide capture and utilization: state of the art and future challenges, Chem. Soc. Rev. 49 (2020) 8584–8686.
- [2] Y. Yang, Z. Ren, S. Zhou, M. Wei, Perspectives on multifunctional catalysts derived from layered double hydroxides toward upgrading reactions of biomass resources, ACS Catal. 11 (2021) 6440–6454.
- [3] L. Lei, Y. Wang, Z. Zhang, J. An, F. Wang, Transformations of biomass, its derivatives, and downstream chemicals over ceria catalysts, ACS Catal. 10 (2020) 8788–8814.
- [4] P. Zhou, Y. Chen, P. Luan, X. Zhang, Z. Yuan, S.-X. Guo, Q. Gu, B. Johannessen, M. Mollah, A.L. Chaffee, D.R. Turner, J. Zhang, Selective electrochemical hydrogenation of furfural to 2-methylfuran over a single atom Cu catalyst under mild pH conditions, Green Chem. 23 (2021) 3028–3038.
- [5] J.-P. Lange, E. vanderHeide, J. vanBuijtenen, R. Price, Furfural-a promising platform for lignocellulosic biofuels, ChemSusChem 5 (2012) 150–166.
- [6] C. Xu, E. Paone, D. Rodríguez-Padrón, R. Luque, F. Mauriello, Recent catalytic routes for the preparation and the upgrading of biomass derived furfural and 5-hydroxymethylfurfural, Chem. Soc. Rev. 49 (2020) 4273–4306.
- [7] A. Mazar, O. Ajao, M. Benali, N. Jemaa, W. Wafa Al-Dajani, M. Paleologou, Integrated multiproduct biorefinery for furfural production with acetic acid and lignin recovery: design, scale-up evaluation, and technoeconomic analysis, ACS Sustain, Chem. Eng. 8 (2020) 17345–17358.
- [8] X. Li, P. Jia, T. Wang, Furfural: A promising platform compound for sustainable production of C<sub>4</sub> and C<sub>5</sub> chemicals, ACS Catal. 6 (2016) 7621–7640.
- [9] C.P. Jiménez-Gómez, J.A. Cecilia, D. Durán-Martín, R. Moreno-Tost, J. Santamaría-González, J. Mérida-Robles, R. Mariscal, P. Maireles-Torres, Gasphase hydrogenation of furfural to furfuryl alcohol over Cu/ZnO catalysts, J. Catal. 336 (2016) 107–115.
- [10] K. Fulajtárova, T. Soták, M. Hronec, I. Vávra, E. Dobročka, M. Omastová, Aqueous phase hydrogenation of furfural to furfuryl alcohol over Pd-Cu catalysts, Appl. Catal. A-Gen. 502 (2015) 78–85.
- [11] M.J. Taylor, S.K. Beaumont, M.J. Islam, S. Tsatsos, C.A.M. Parlett, M.A. Issacs, G. Kyriakou, Atom efficient PtCu bimetallic catalysts and ultra dilute alloys for the selective hydrogenation of furfural, Appl. Catal. B. 284 (2021) 119737.
- [12] S. Bai, L. Bu, Q. Shao, X. Zhu, X. Huang, Multicomponent Pt-based zigzag nanowires as selectivity controllers for selective hydrogenation reactions, J. Am. Chem. Soc. 140 (2018) 8384–8387.
- [13] H. Wang, S. Bai, Y. Pi, Q. Shao, Y. Tan, X. Huang, A strongly coupled ultrasmall  $Pl_3Co$  nanoparticle-ultrathin  $Co(OH)_2$  nanosheet architecture enhances selective hydrogenation of  $\alpha$ ,  $\beta$ -unsaturated aldehydes, ACS Catal. 9 (2019) 154–159.
- [14] Y. Cao, B. Chen, J. Guerrero-Sánchez, I. Lee, X. Zhou, N. Takeuchi, F. Zaera, Controlling selectivity in unsaturated aldehyde hydrogenation using singlesite alloy catalysts, ACS Catal. 9 (2019) 9150–9157.
- [15] J. Li, M. Žahid, W. Sun, X. Tian, Y. Zhu, Synthesis of Pt supported on mesoporous g-C<sub>3</sub>N<sub>4</sub> modified by ammonium chloride and its efficiently selective hydrogenation of furfural to furfuryl alcohol, Appl. Surf. Sci. 528 (2020) 146983.
- [16] M. Zahid, J. Li, A. Ismail, F. Zaera, Y. Zhu, Platinum and cobalt intermetallic nanoparticles confined within MIL-101(Cr) for enhanced selective hydrogenation of the carbonyl bond in α, β-unsaturated aldehydes: synergistic effects of electronically modified Pt sites and Lewis acid sites, Catal. Sci. Technol. 11 (2021) 2433–2445.
- [17] W. Zhang, W. Shi, W. Ji, H. Wu, Z. Gu, P. Wang, X. Li, P. Qin, J. Zhang, Y. Fan, T. Wu, Y. Fu, W. Zhang, F. Huo, Microenvironment of MOF channel coordination with Pt NPs for selective hydrogenation of unsaturated aldehydes, ACS Catal. 10 (2020) 5805–5813.
- [18] X. Meng, Y. Yang, L. Chen, M. Xu, X. Zhang, M. Wei, A control over hydrogenation selectivity of furfural via tuning exposed facet of Ni catalysts, ACS Catal. 9 (2019) 4226–4235.
- [19] Y. Yang, L. Chen, Y. Chen, W. Liu, H. Feng, B. Wang, X. Zhang, M. Wei, The selective hydrogenation of furfural over intermetallic compounds with outstanding catalytic performance, Green Chem. 21 (2019) 5352–5362.
- [20] P. Jia, X. Lan, X. Li, T. Wang, Highly active and selective NiFe/SiO<sub>2</sub> bimetallic catalyst with optimized solvent effect for the liquid-phase hydrogenation of furfural to furfuryl alcohol, ACS Sustain Chem. Eng. 6 (2018) 13287–13295.
- [21] C. Wang, Y. Liu, Z. Cui, X. Yu, X. Zhang, Y. Li, Q. Zhang, L. Chen, L. Ma, In situ synthesis of Cu nanoparticles on carbon for highly selective hydrogenation of furfural to furfuryl alcohol by using pomelo peel as the carbon source, ACS Sustain Chem. Eng. 8 (2020) 12944–12955.
- [22] M.J. Islam, M. Granollers Mesa, A. Osatiashtiani, M.J. Taylor, J.C. Manayil, C.M.A. Parlett, M.A. Isaacs, G. Kyriakou, The effect of metal precursor on copper phase dispersion and nanoparticle formation for the catalytic transformations of furfural, Appl. Catal. B. 273 (2020) 119062.

- [23] S. Thongratkaew, C. Luadthong, S. Kiatphuengporn, P. Khemthong, P. Hirunsit, K. Faungnawakij, Cu-Al spinel-oxide catalysts for selective hydrogenation of furfural to furfuryl alcohol, Catal. Today. 367 (2021) 177–188.
- [24] F. Tang, L. Wang, M. Dessie Walle, A. Mustapha, Y.-N. Liu, An alloy chemistry strategy to tailoring the d-band center of Ni by Cu for efficient and selective catalytic hydrogenation of furfural, J. Catal. 383 (2020) 172–180.
- [25] Z. Fu, Z. Wang, W. Lin, W. Song, S. Li, High efficient conversion of furfural to 2-methylfuran over Ni-Cu/Al<sub>2</sub>O<sub>3</sub> catalyst with formic acid as a hydrogen donor, Appl. Catal. A-Gen. 547 (2017) 248–255.
- [26] Y. Yang, Z. Du, Y. Huang, F. Lu, F. Wang, J. Gao, J. Xu, Conversion of furfural into cyclopentanone over Ni-Cu bimetallic catalysts, Green Chem. 15 (2013) 1932– 1940.
- [27] R.T. Hannagan, G. Giannakakis, M. Flytzani-Stephanopoulos, E.C.H. Sykes, Single-atom alloy catalysis, Chem. Rev. 120 (2020) 12044–12088.
- [28] P. Xiao, J. Zhu, D. Zhao, Z. Zhao, F. Zaera, Y. Zhu, Porous LaFeO<sub>3</sub> prepared by an in situ carbon templating method for catalytic transfer hydrogenation reactions, ACS Appl. Mater. Interfaces. 11 (2019) 15517–15527.
- [29] D. Hu, W. Fan, Z. Liu, L. Li, Three-Dimensionally hierarchical Pt/C nanocomposite with ultra-high dispersion of Pt nanoparticles as a highly efficient catalyst for chemoselective cinnamaldehyde hydrogenation, ChemCatChem 10 (2018) 779–788.
- [30] M. Liu, L. Yuan, G. Fan, L. Zheng, L. Yang, F. Li, NiCu nanoparticles for catalytic hydrogenation of biomass-derived carbonyl compounds, ACS Appl. Nano Mater. 3 (2020) 9226–9237.
- [31] Y. Tong, Y. Li, Z. Li, P. Wang, Z. Zhang, X. Zhao, F. Yuan, Y. Zhu, Influence of Sm on the low temperature NH<sub>3</sub>-SCR of NO activity and H<sub>2</sub>O/SO<sub>2</sub> resistance over the  $Sm_aMnNi_2Ti_7O_x$  (a = 0.1, 0.2, 0.3, 0.4) catalysts, Appl. Catal. A-Gen. 590 (2020) 117333.
- [32] S. Ali, L. Chen, Z. Li, T. Zhang, R. Li, S.u.H. Bakhtiar, X. Leng, F. Yuan, X. Niu, Y. Zhu, Cu<sub>x</sub>-Nb<sub>1.1-x</sub> (x = 0.45, 0.35, 0.25, 0.15) bimetal oxides catalysts for the low temperature selective catalytic reduction of NO with NH<sub>3</sub>, Appl. Catal. B. 236 (2018) 25-35.
- [33] X. Liu, X. Wu, D. Weng, Z. Si, R. Ran, Evolution of copper species on Cu/SAPO-34 SCR catalysts upon hydrothermal aging, Catal. Today. 281 (2017) 596–604.
- [34] J. He, L. Schill, S. Yang, A. Riisager, Catalytic Transfer Hydrogenation of Bio-Based Furfural with NiO Nanoparticles, ACS Sustain. Chem. Eng 6 (2018) 17220–17229.
- [35] Z. Pan, H. Jiang, B. Gong, R. Luo, W. Zhang, G.-H. Wang, Layered double hydroxide derived NiAl-oxide hollow nanospheres for selective transfer hydrogenation with improved stability, J. Mater. Chem. A 8 (2020) 23376– 23384
- [36] X. Yang, W. Liu, F. Tan, Z. Zhang, X. Chen, T. Liang, C. Wu, A robust strategy of homogeneously hybridizing silica and Cu<sub>3</sub>(BTC)<sub>2</sub> to in situ synthesize highly dispersed copper catalyst for furfural hydrogenation, Appl. Catal. A-Gen. 596 (2020) 117518.
- [37] R. Wang, H. Liu, X. Wang, X. Li, X. Gu, Z. Zheng, Plasmon-enhanced furfural hydrogenation catalyzed by stable carbon-coated copper nanoparticles driven from metal-organic frameworks, Catal. Sci. Technol. 10 (2020) 6483–6494.
- [38] K.W. Golub, T.P. Sulmonetti, L.A. Darunte, M.S. Shealy, C.W. Jones, Metalorganic-framework-derived Co/Cu-carbon nanoparticle catalysts for furfural hydrogenation, ACS Appl. Nano. Mater. 2 (2019) 6040–6056.

- [39] Y. Zhu, X. Kong, B. Peng, L. Li, Z. Fang, Y. Zhu, Efficient Cu catalyst for 5-hydroxymethylfurfural hydrogenolysis by forming Cu-O-Si bonds, Catal. Sci. Technol. 10 (2020) 7323–7330.
- [40] G. Cui, X. Zhang, H. Wang, Z. Li, W. Wang, Q. Yu, L. Zheng, Y. Wang, J. Zhu, M. Wei, ZrO<sub>2-x</sub> modified Cu nanocatalysts with synergistic catalysis towards carbon-oxygen bond hydrogenation, Appl. Catal. B. 280 (2021) 119406.
- [41] J.B. Joo, R. Dillon, I. Lee, Y. Yin, C.J. Bardeen, F. Zaera, Promotion of atomic hydrogen recombination as an alternative to electron trapping for the role of metals in the photocatalytic production of H<sub>2</sub>, P. Natl. Acad. Sci. USA 111 (2014) 7942–7947.
- [42] R. Rao, A. Dandekar, R.T.K. Baker, M.A. Vannice, Properties of copper chromite catalysts in hydrogenation reactions, J. Catal. 171 (1997) 406–419.
- [43] D. Liu, D. Zemlyanov, T. Wu, R.J. Lobo-Lapidus, J.A. Dumesic, J.T. Miller, C.L. Marshall, Deactivation mechanistic studies of copper chromite catalyst for selective hydrogenation of 2-furfuraldehyde, J. Catal. 299 (2013) 336–345.
- [44] H. Zhang, C. Canlas, A. Jeremy Kropf, J.W. Elam, J.A. Dumesic, C.L. Marshall, Enhancing the stability of copper chromite catalysts for the selective hydrogenation of furfural with ALD overcoating (II)-Comparison between TiO<sub>2</sub> and Al<sub>2</sub>O<sub>3</sub> overcoatings, J. Catal. 326 (2015) 172–181.
- [45] V.S. Marakatti, N. Arora, S. Rai, S.C. Sarma, S.C. Peter, Understanding the role of atomic ordering in the crystal structures of Ni<sub>x</sub>Sn<sub>y</sub> toward efficient vapor phase furfural hydrogenation, ACS Sustain. Chem. Eng. 6 (2018) 7325–7338.
- [46] H. Zhang, J. Dong, X. Qiao, J. Qin, H. Sun, A. Wang, L. Niu, G. Bai, In-situ generated highly dispersed nickel nanoclusters confined in MgAl mixed metal oxide platelets for benzoic acid hydrogenation, J. Catal. 372 (2019) 258–265.
- [47] D. Shi, J.M. Vohs, Deoxygenation of biomass-derived oxygenates: reaction of furfural on Zn-modified Pt(111), ACS Catal. 5 (2015) 2177–2183.
- [48] H. Daly, H.G. Manyar, R. Morgan, J.M. Thompson, J.J. Delgado, R. Burch, C. Hardacre, Use of short time-on-stream attenuated total internal reflection infrared spectroscopy to probe changes in adsorption geometry for determination of selectivity in the hydrogenation of citral, ACS Catal. 4 (2014) 2470–2478.
- [49] P. Koley, S. Chandra Shit, B. Joseph, S. Pollastri, Y.M. Sabri, E.L.H. Mayes, L. Nakka, J. Tardio, J. Mondal, Leveraging Cu/CuFe<sub>2</sub>O<sub>4</sub>-catalyzed biomass-derived furfural hydrodeoxygenation: a nanoscale metal-organic-framework template is the prime key, ACS Appl. Mater. Interfaces. 12 (2020) 21682–21700.
- [50] B. Chen, F. Zaera, Hydrogenation of cinnamaldehyde on Cu(110) single-crystal surfaces, J. Phys. Chem. C. 125 (2021) 14709–14717.
- [51] M.T. Nayakasinghe, J. Guerrero-Sanchez, N. Takeuchi, F. Zaera, Adsorption of crotonaldehyde on metal surfaces: Cu vs Pt, J. Chem. Phys. 154 (2021).
- [52] S. Chen, R. Wojcieszak, F. Dumeignil, E. Marceau, S. Royer, How catalysts and experimental conditions determine the selective hydroconversion of furfural and 5-hydroxymethylfurfural, Chem. Rev. 118 (2018) 11023–11117.
- [53] Y. Shi, Y. Zhu, Y. Yang, Y.-W. Li, H. Jiao, Exploring furfural catalytic conversion on Cu(111) from computation, ACS Catal. 5 (2015) 4020–4032.
- [54] S. Sitthisa, T. Sooknoi, Y. Ma, P.B. Balbuena, D.E. Resasco, Kinetics and mechanism of hydrogenation of furfural on Cu/SiO<sub>2</sub> catalysts, J. Catal. 277 (2011) 1–13.